

Electrocuting Grids and the Sensing of Insect Wing-beats: Initial Results

Brendan Khoo T. T.*, Muralindran M.***, Rosalyn R. P.***, W. W. Kitt****

**(Faculty of Engineering, Universiti Malaysia Sabah, Jalan UMS, 88400, Kota Kinabalu, Sabah, Malaysia*

** *(Faculty of Engineering, Universiti Malaysia Sabah, Jalan UMS, 88400, Kota Kinabalu, Sabah, Malaysia*

*** *(Faculty of Engineering, Universiti Malaysia Sabah, Jalan UMS, 88400, Kota Kinabalu, Sabah, Malaysia*

**** *(Department of Electrical and Computer Engineering, Curtin University, Miri Sarawak, Malaysia*

ABSTRACT

Automated real-time insect classification could be the key to solving pest insect problems that plague our daily lives. In recent years, optical wing-beat sensors have been one of the main staples for wing-beat based insect species classification. These works commonly utilize the wing-beat or wing-flap characteristics acquired from photodiodes to predict the species and types of insect via modern classification techniques. However, instead of utilizing the established optical-based method, this paper further explores the novel capacitive sensor concept for sensing insect wing-beats. The proposed method uses the electrocuting grids of the insect zapper as the sensing elements for detecting insect wing-beats. This sensing method introduces a new possibility in utilizing electrocuting grids to selectively kill insects of a specific species or types, while performing as a surveillance tool. This paper highlights the expansion of the initial capacitive wing-beat sensor concept through further integration with the high-voltage supply of the electrocuting trap.

Keywords - Capacitive Sensor, Electrocuting Traps, Insect Species Recognition, Insect Surveillance, Insect Trap, Intelligent Trap, Smart Trap, Wing-beat Sensor

Date of Submission: 20-08-2020

Date of Acceptance: 06-09-2020

I. INTRODUCTION

The early efforts to understanding and measuring insect wing-beats can be traced as far back as the 1867 when Landois attempted to measure insect wing-beats by matching the flight-tone to a tuning fork of known frequency after Mühlhäuser, a year before, suggested the link between flight-tone and wing-beats [1]. This attempt was superseded by other early methods, notably, Wheatstone kaleidophone, kymograph, high speed photography and stroboscope, but had limited usefulness due to their recording and speed limitations [2]. The advancement in electronics and acoustic devices such as microphones, headphones and even gramophone had opened possibilities to better solutions in measuring and recording the wing-beats of the insects [1], [3]–[5]. Although these methods had overcome prior recording problems, the early acoustic (microphone) methods still require complex sound-proofing, and the gramophone method still requires the insects to be tethered.

Lately, most wing-beat-based insect species identification research have been centering around optical detectors (photo-sensor), mainly, due to their simplicity, low cost and good signal to noise ratio (SNR). This photo-detector concept can be credited

to Richards [6], whom, noticed and recorded the signal burst when an insect flew in the path of the sunlight to the red-sensitive cesium photoelectric cell. This original work has greatly improved by replacing the photosensor and including an artificial light source: halogen lamp [7], laser [8], [9] and LED [10], [11].

The discovery of the optical sensing method has revolutionized the insect wing-beat recording methodology and has spurred the automated insect species recognition field. One of the popular setups used by researchers is the low-cost laser apparatus introduced in [8]. This low-cost and straightforward apparatus functions by reflecting the laser beam from a laser diode back to the photo-transistor (placed beside the laser) with a mirror. The wing movement of the insect passing the beam will slightly occlude the laser, thus, generating wing-beat signal that is then filtered and amplified by the circuit board before digitization.

This setup and its variants were used in several works to study different algorithms for species recognition including Dynamic Time Warping-Delta (DTW-D) [12], Bayesian [13], Dynamic Time Warping (DTW) with nonlinear median filtering (NMF) [14], Mel-Frequency Cepstral Coefficients (MFCC) with SVM-RBF [15],

robust stacked autoencoder (R-SAE) with SVM [16] and kernel adaptive autoregressive-moving average (KAARMA) [17]. A noise immune solution for laser wing-beat sensor has been described in [9] by incorporating fixed frequency modulation to the laser source, as well as, a demodulation circuitry at the receiver side. The mentioned design helps to reject the mains frequency and harmonics noise emitted by the indoor artificial lighting [9]. A year later, these authors presented an improved 2D wing-beat sensor with a 20 photodiode array (2 x 10) receiver and an 8 infrared (IR) LED array (2 x 4) emitter [10], [18], [19] instead of a single photosensor or a linear array sensor like the ones in [7], [16]. This is to provide a larger field of view for capturing full wingbeat motion and fast flying insects.

In this paper, a different approach of acquiring mosquito wing-beats will be introduced. The technique discussed here is an improvement and an expansion of the novel capacitive wing-beat sensor proposed in [20]. The capacitive wing-beat sensor was introduced as a potential alternative to conventional optical wing-beat sensor that could spur the implementation of intelligent insect traps into our daily life via commercial electrocuting traps. However, unlike our prior wing-beat sensing concept in [20] that isolates the capacitive sensor from the high voltage circuit physically through a high-voltage relay, the system discussed here integrates the capacitive sensing circuit with the high-voltage circuitry to achieve a more unified and practical design.

II. INTELLIGENT MOSQUITO TRAP

Similar to our prior work, the envisioned system of this paper consists of a capacitive sensor module, an embedded processor, an analog-to-digital converter and a wireless internet module (cellular or Wi-Fi). The system in this paper however, introduces an additional component, a controllable high-voltage supply which acts as an electrocution power source as well as an excitation source for the capacitive wing-beat sensor. As shown in Fig. 1, the capacitive sensor module is connected directly to the electrocuting grid of the commercial insect trap to actively measure the capacitance change in the grids using the high-voltage supply as the excitation source. While idling, the high-voltage supply outputs minimum voltage just to excite the capacitive wing-beat sensor. This will significantly lower down the power consumption of the high-voltage circuit, aside from preventing the electrocuting grids from electrocuting non-target insects. The analog signal output of the capacitive sensor module is then digitized via an analog-to-digital converter for the embedded processor. The embedded processor

computes the capacitive data and determines (according to the capacitive wing-beat signal) to either ignore or electrocute the approaching insect by increasing the output voltage of the high-voltage supply. The overall operation of the system can be monitored, logged and controlled remotely via the internet connection provided by the cellular/Wi-Fi module.

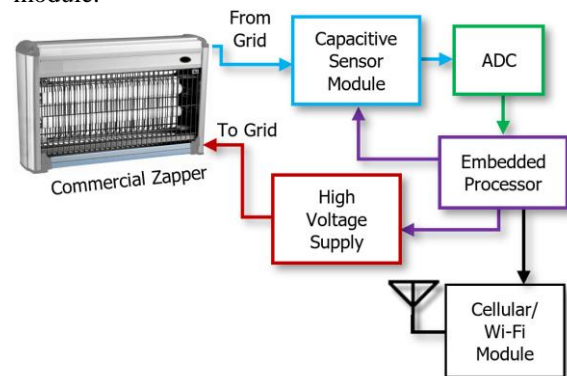


Fig. 1. The proposed concept

Fig. 1 describes the potential implementation of the proposed system, although, the scope of this paper will only cover the design and development of the capacitive sensor module and high-voltage supply involved in acquiring the mosquito wing-beat signal. The following sections of this paper will elaborate on the design and development of the capacitive sensing module and high-voltage supply. They then tested with live mosquito samples to obtain the preliminary result of the proposed contraption.

III. THE SENSOR AND TRAPPING MECHANISM

The proposed system in this paper features the development of the capacitive wing-beat sensor module and the high voltage supply. By utilizing the similar electrocuting grids described in [20], the operation of the core components in this paper can be summarized as Fig. 2. The electrocuting grids are conductive rods positioned in parallel to form a plane where the ends of alternate rods are wired together, creating two sets of interlacing electrodes: transmit and receive. On the transmitting side, the electrodes are excited by the high voltage supply directly. The high voltage supply is a high-frequency, high-voltage resonant inverter that outputs fixed-frequency sinusoidal-signal. The output voltage of the inverter can be controlled to achieve a desirable excitation level for the capacitive sensor.

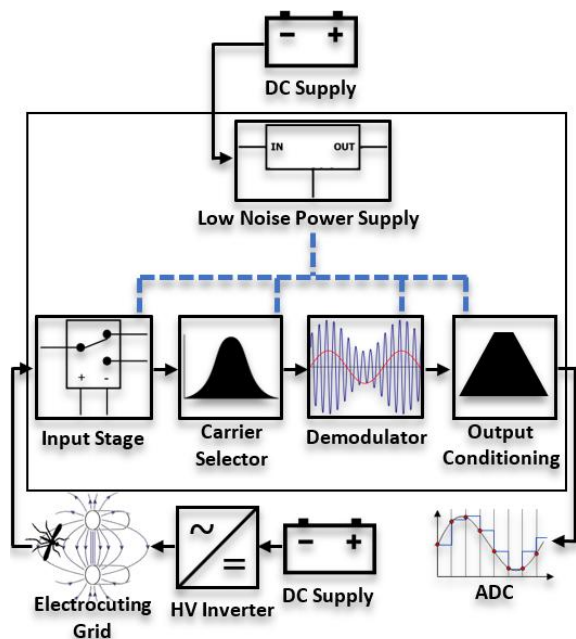


Fig. 2. The main stages of the proposed system

At the receiving side, the receive electrodes are connected to the input stage. The input stage selects the appropriate sensing resistance for high-voltage (electrocution) and low-voltage (wing-beat sensing) operations. Low-voltage operation is the idling mode where the input stage actively buffers the coupled excitation signal for the carrier selector circuit. The amplitude of the coupled excitation signal varies according to the capacitance of the electrocuting grids, which in this case, influenced by the wing-beats of a nearby insect. The carrier selector circuit removes out-of-band noise and signals that are coupled through the receive electrodes such as noise from nearby power-line, electronic devices and radio transmitters.

The minute amplitude fluctuations caused by the insect wing-beats are extracted by the AM demodulator circuit. The demodulated signal is then amplified and band-pass filtered to target only the wing-beat frequencies and the harmonics of most common mosquitoes (150Hz – 2000Hz) via the output conditioning circuit. This circuit conditions the signal for digitization by an ADC for further processing by the embedded processor. Fig. 2 illustrates the overall flow of the stages mentioned.

3.1 High Voltage Supply (Sensor Excitation Source)

The development of the inverter circuit for the high voltage AC supply is based on the high-voltage high-frequency transformer – TLE2803. Although the transformer is built primarily for use in a Royer topology, the switching of the inverter circuit is controlled with an external microcontroller.

This is because the inverter circuit must operate at a very stable and accurate frequency when functioning as the sensor excitation source. This microcontroller is supplied with a stable and accurate reference clock from either a crystal unit, a crystal oscillator or a phase-lock-loop (PLL) to ensure a reliable, low-jitter and accurate MOSFET gate signals.

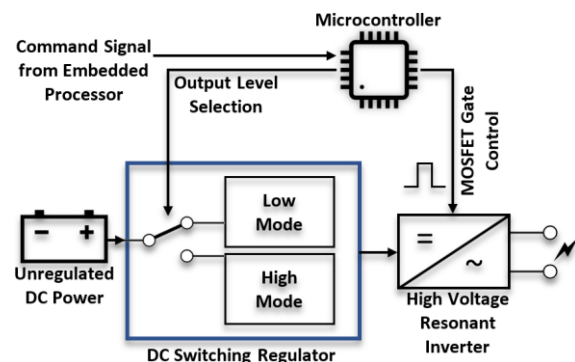


Fig. 3. High voltage supply

The inverter controller circuit is based on DSPIC33EV256GM102 – a 16-bit digital signal controller by Microchip Technology. The DSPIC33EV256GM102 controller operates on a 5VDC supply to adequately trigger the gates of the switching MOSFET in the high voltage resonant inverter circuit. This digital-signal-controller works as a slave device and receive command from the embedded processor, and executes commands including change output voltage and enabling/disabling PWM output as shown in Fig. 3. These commands are received via the SPI lines from the main sensor controller. The four PWM output lines shown in Fig. 4 are coming from two separate high-speed PWM modules (PWM1 and PWM2) for controlling two sets of switching MOSFETs. These high-speed outputs are used to drive the gates of the switching MOSFETs in the high voltage resonant inverter directly. The system clock of this microcontroller is derived from a 4.096MHz crystal unit. This crystal frequency is selected to accurately achieve a switching frequency of 455.111kHz for the resonant inverter to match the center-frequency of the carrier selector circuit.

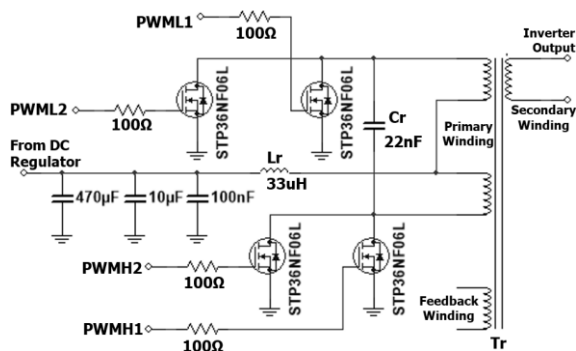


Fig. 4. Resonant inverter circuit

3.2 Electrocuting Grid (Sensing Electrodes)

The electrocuting grids or sensing electrodes used in this paper are 1.8 mm conductive stainless-steel rods. The electrodes are secured with two High-Density Polyethylene (HDPE) brackets at both ends and are spaced equally at 8 mm apart. As shown in Fig. 5, the transmit and receive electrodes are placed alternately in a plane and are connected in parallel with connector blocks.

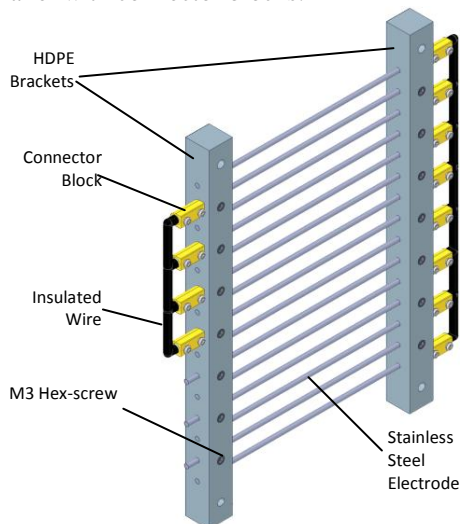


Fig. 5. Electrocuting grids (sensing electrodes)

3.3 Capacitive Wing-beat Sensor

3.3.1 Input Stage

This sub-circuit connects directly to the “receive side” of the electrocuting grids, thus, it must be able to handle the weak capacitive sensing signal as well as the high-voltage event during the electrocution of an insect. For that reason, it consists of two input resistors, sensing resistor R_S and bypass resistor R_{S2} , that are selectable by the relay S_1 . S_1 is a G6K2FYDC5BYOMR relay from Omron – a high-frequency, low-insertion-loss, electromechanical-relay. The bypass resistor R_{S2} , having a low resistance, is normally isolated from the input during the idling or wing-beat sensing mode. The S_1 swiftly connects R_{S2} to the input before allowing the high-voltage supply to operate at high-voltage mode, thus,

bypassing the R_S to protect the preamplifier from high-voltage input.

The input of this sub-circuit is further protected by two back-to-back transient-voltage-suppressor (TVS) diodes – ESD9R3.3ST5G. These diodes clamp the input to around $\pm 7.8V_{peak}$ when subjected to a pulse current of 1A. This protection strategy allows repeated high-voltage surges at the circuit input without any significant degradation in the event of a short-circuit between the electrocuting grids or an external electrical transient. The ESD9R3.3ST5G is chosen for this application because of its low capacitance (0.5 pF), high speed response (below 1 ns), very low leakage current (below 1 nA) and low clamping voltage.

The LNA selected for this circuit is AD8066, the dual amplifier version of AD8065, an FET op-amp from Analog Devices Inc. This amplifier is selected specifically for its low-cost, low input noise ($7nV/\sqrt{Hz}$ and $0.6 fA/\sqrt{Hz}$), low input bias current (1 pA), high slew rate ($180 V/\mu s$), low input-capacitance (4.5pF), low input-impedance ($1T\Omega$) and high band-width ($42MHz @ 2V_{pp}$).

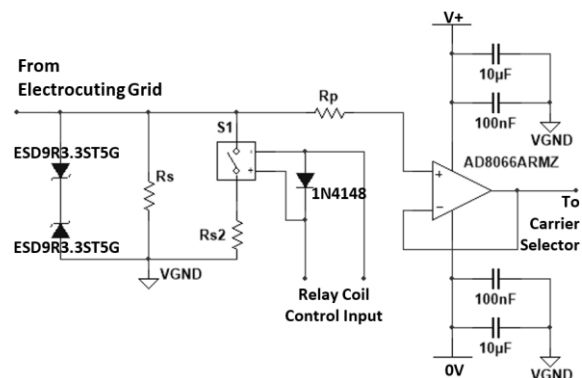


Fig. 6. Input Stage

3.3.2 Carrier Selector

This stage removes all out-of-band signals and noise from the input signal, and only allows a narrowband signal that centers at the frequency of the excitation source. Unlike the tuner stage in our previous paper [20], this design has lower complexity, smaller size, lower noise, more precise and stable center frequency, and higher Q-factor or selectivity. On the downside, the carrier frequency of this circuit cannot be tuned and can only use the frequencies of common discriminators (455 kHz, 5.5 MHz and 10.7 MHz).

As demonstrated in the schematic Fig. 7, the output from the input stage is fed through a CFWLB455KEFA ceramic discriminator/filter, before buffering by the second channel of the AD8066 LNA. The CFWLB455KEFA is a ceramic filter by Murata with six integrated piezoelectric elements to form a 15kHz bandpass filter (6dB) that

centers at 455 kHz. This 15kHz bandwidth could sufficiently allow a baseband signal (insect wing-beat signal) up to 7.5kHz at 6dB attenuation. The output of this stage (AD8066 buffer) is then passed to the demodulation circuit. The stop-band of CFWLB455KEFA ceramic discriminator is rated at 455 ± 100 kHz, where outside this band, signals and noise are attenuated below -35dB.

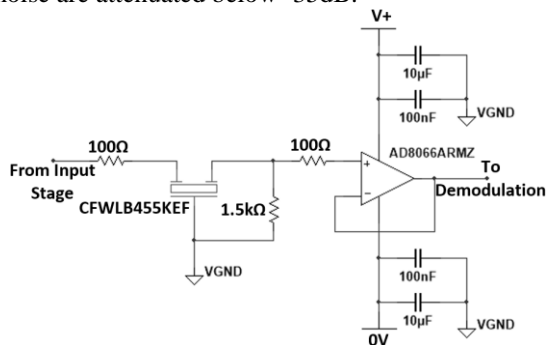


Fig. 7. Carrier selector circuit

3.3.3 Demodulation

The demodulation circuit of the capacitive wing-beat sensor extracts the changes in capacitance at the electrocuting grids from the input signal by tracking the amplitude variation or amplitude modulation of the excitation signal. This can be done accurately with a precision rectifier circuit. This research employs an AD8036 clamp amplifier circuit as a low-cost, high-speed, high-precision and full-wave solution for precision rectification. Fig. 8 shows the full-wave rectifier circuit and two stages of RLC filters to remove the carrier components before passing the signal to output conditioning circuit.

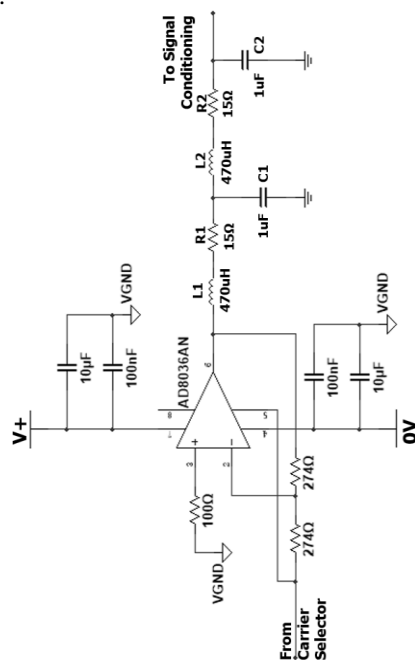


Fig. 8. AM demodulator circuit

3.3.4 Output Conditioning

The minute capacitance fluctuation caused by the insect wing-flap modulates the excitation signal in a very small degree, hence, a band-pass with large amplification is needed to correctly amplify the spectrum of interest while suppressing the out-of-band signals. First of all, at the low-side, the band-pass must eliminate the common 50Hz mains frequency. This is important to prevent saturation of the op-amps in the output conditioning circuit. At the high-side, the cut-off frequency is set to 2kHz to accommodate most of the insect-wing-beat signal harmonics.

In this circuit, the capacitive wing-beat signal extracted by the demodulation stage is filtered, amplified and conditioned for the ADC converter. This is done via a four-stage, 8th order active wide band-pass filter. These filter stages are implemented on a single quad-amplifier IC, OPA1604. OPA1604 is a high-fidelity audio operation amplifier with very low input noise density (2.5nV/ $\sqrt{\text{Hz}}$ at 1kHz), very high GBW product (35 MHz minimum), very low distortion (THD+N = 0.00003%), high open-loop gain (140dB when loaded with 2k Ω) and low input-bias current (20nA).

This band-pass filter follows Type-I-Chebyshev frequency response with characteristics of each stage listed in

Table 1. These parameters are tuned to achieve a low-side frequency response of 50Hz/150Hz (stop-band/cut-off) and 2kHz/5.6kHz (cut-off/stop-band) at the high-side using a ripple gain of 0.01dB. The overall total amplification of 10000V/V is attained to maximize the signal resolution for interfacing with the ADC.

Table 1. Active filter circuit parameters

Stage	Gain (V/V)	Pass-band (Hz)	Q
1	5.77	155	1.72
2	5.77	1930	1.72
3	17.3	193	0.575
4	17.3	1550	0.575

Fig. 9 displays the schematic of the active band-pass filters responsible for shaping/conditioning the output for the ADC.

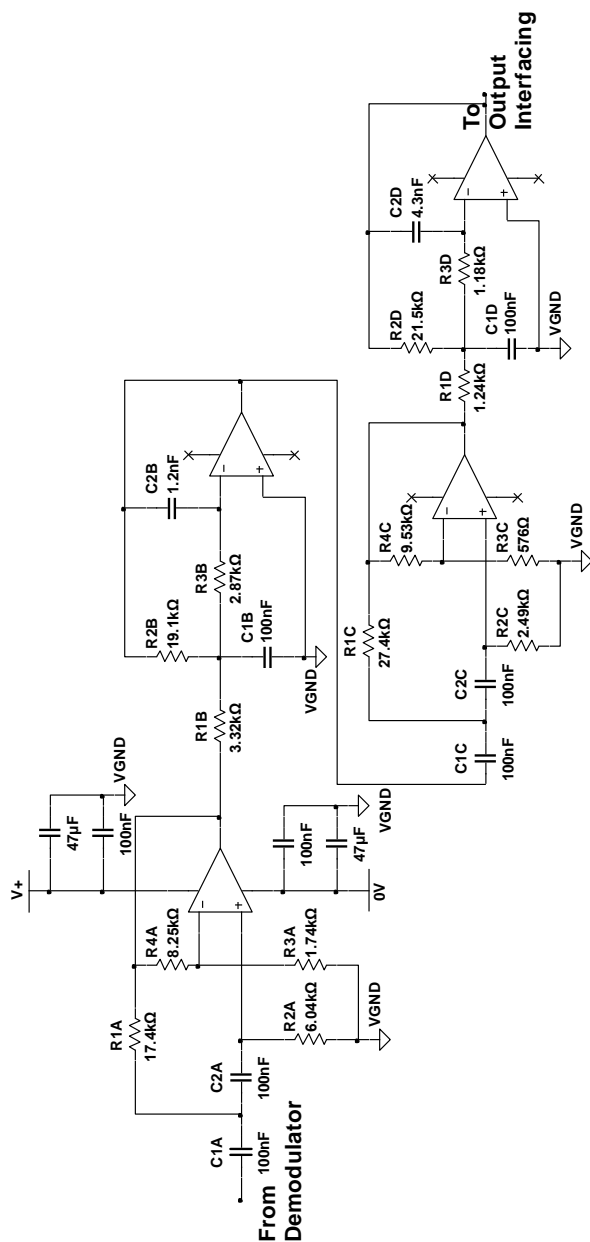


Fig. 9. Output conditioning circuit

IV. EXPERIMENT

4.1 Test Chamber

The test chamber is an important tool built for providing a flexible and convenient way to insert insect samples, in a standard laboratory/medical plastic container, into a confined chamber where the sample is able to fly and interact with the electrocuting grids unimpeded. The detailed specifications and design of the test chamber are described in [20]. Shown in Fig. 10 is the test chamber assembled with the electrocuting grids.

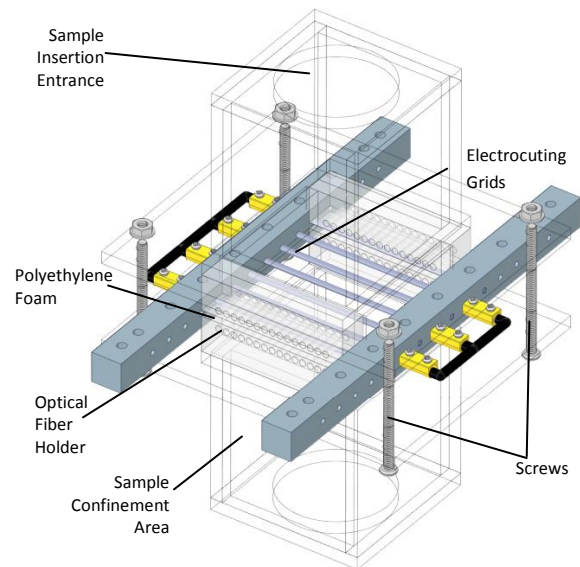


Fig. 10. Test chamber assembled with electrocuting grids

4.2 Capacitive Sensing Circuit

The proposed capacitive wing-beat sensor circuit is developed on a four-layer PCB as shown in Fig. 11. It can be powered with an unregulated DC supply as it is equipped with an on-board low-noise voltage regulator and a virtual ground buffer to produce 3 power rails: positive rail (+10V), virtual ground (+5V) and negative rail (0V).

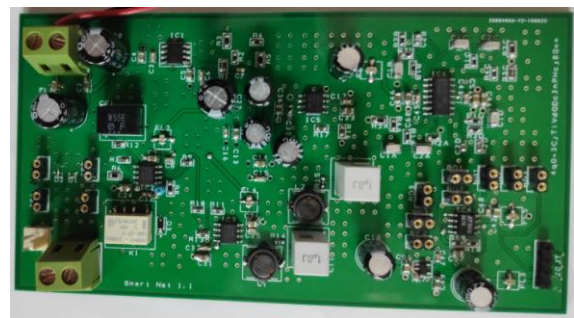


Fig. 11. The fabricated circuit of the proposed capacitive sensor

4.3 High Voltage Supply Circuit

The high voltage supply circuit is developed on a four-layer PCB to handle the high current load of the high-voltage resonant inverter and the selectable voltage source. As seen in Fig. 12, the DC switching regulators, the high voltage resonant inverter and the digital signal controller are located at: the bottom left, bottom right and top left respectively.



Fig. 12. The fabricated circuit of the proposed High Voltage Supply

4.4 Experimental Setup

The experimental setup used for testing the proposed system is comprised of a 3-cell lithium polymer battery to power the high-voltage supply and capacitive wing-beat sensor circuit. The output of the high voltage supply is connected to the transmit side of the electrocuting grids. The receive side of the electrocuting grids are wired to the input of the capacitive wing-beat sensor circuit. The output of the sensor circuit is then passed to PCM1808 – a 24-bit audio ADC. This audio ADC is controlled by the PIC32MZ2048EFH100 microcontroller of the “Clicker 2” development board via I2S serial protocol. The acquired digital wing-beat signals are lastly recorded and stored in a computer via USB. Fig. 13 summarizes the setup of the experiment.

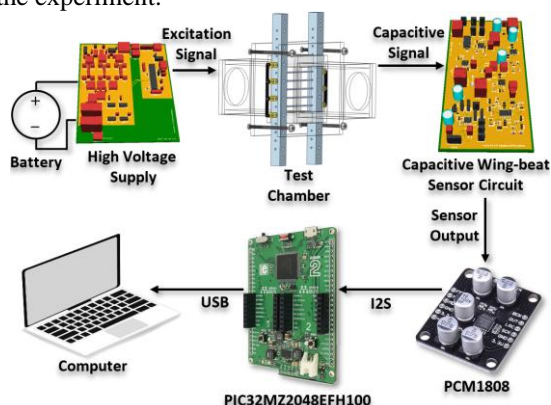


Fig. 13. Overview of the experimental setup
 The actual setup of the experiment is as shown in Fig. 14.

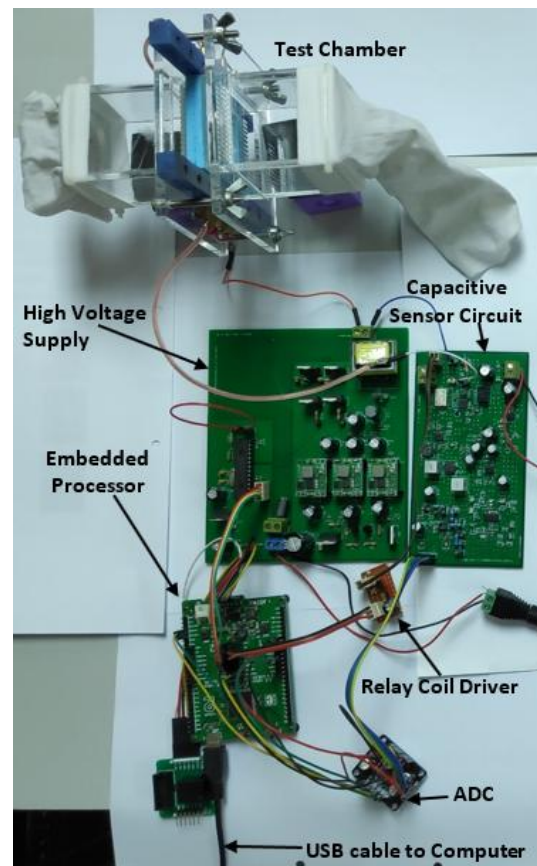


Fig. 14. Experimental setup

V. RESULTS AND DISCUSSION

Two medically important mosquito species, *Aedes albopictus* and *Culex tritaeniorhynchus* are tested with the experimental setup discussed in prior section. These samples are captured locally in the domestic areas around Kota Kinabalu, Sabah. During the experiment, a single sample of each sex and species is inserted and allowed to interact with the electrocuting grids unimpeded, while, the output of the capacitive sensing circuit is consistently recorded at the computer via the USB interface to the embedded processor (PIC32MZ). The recorded data stream is then processed individually to obtain the spectrogram of each mosquito sample type.

The signal samples collected in the experiment are dumped as large text files. These samples are then manually cropped from the large data stream via the spectrograms of the signal analyzer toolbox in MATLAB. Displayed in Fig. 15 is the spectrogram of the cropped capacitive wing-beat signal of a male *Aedes albopictus*. The fundamental frequency of the wing-beats is identified as the spectrum with the highest power. As observed in the plot, the fundamental frequency is around 620Hz and its closest next harmonics are near 1240Hz and 1850Hz.

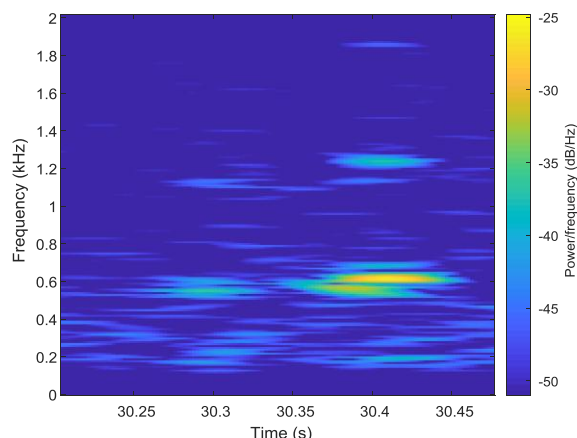


Fig. 15. Wing-beat spectrogram of male *Aedes albopictus*

The fundamental frequency of the capacitive wing-beat signal of a female *Aedes albopictus* sample when darting between the electrocuting grids is clearly discerned to be around 470Hz using the spectrogram in Fig. 16. The closest higher harmonics of these signals are directly above at 930Hz and 1420Hz.

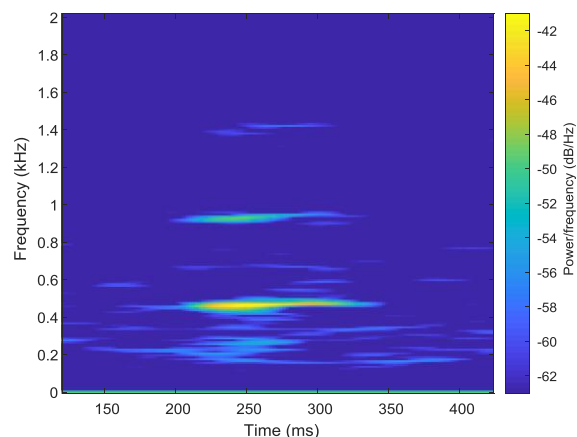


Fig. 16. Wing-beat spectrogram of female *Aedes albopictus*

The spectrogram of the wing-beat signal of a male *Culex tritaeniorhynchus* crossing the electrocuting grids is plotted in Fig. 17. Its fundamental frequency and its next harmonics are observed to be 740 Hz and 1.48 kHz respectively.

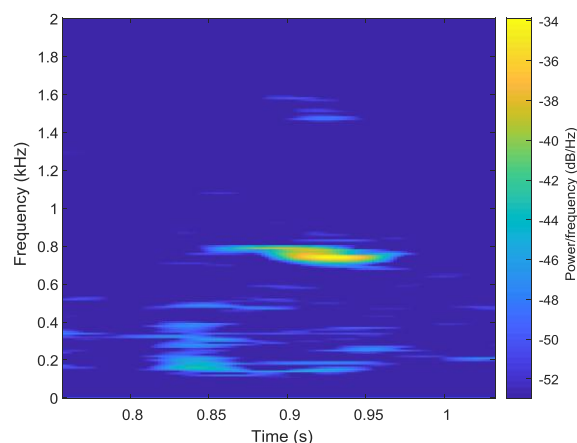


Fig. 17. Wing-beat spectrogram of male *Culex tritaeniorhynchus*

The hovering of a female *Culex tritaeniorhynchus* sample near the electrocuting grids has yielded the spectrogram shown in Fig. 18. The fundamental frequency and the higher harmonics of the wing-beats recorded from the event can be distinguished at 450Hz and 900Hz, 1320Hz respectively.

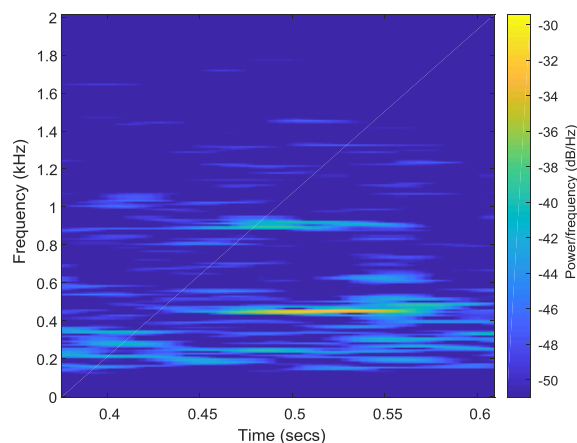


Fig. 18. Wing-beat spectrogram of female *Culex tritaeniorhynchus*

From the results in this section, it is observed that the proposed integration of high-voltage supply (as sensor excitation source) into the capacitive wing-beat sensor has achieved similar sensing outcome as the previous work that utilizes a laboratory waveform generator as the controlled excitation source.

VI. CONCLUSION

This research has further expanded the concept and possibility of creating a low-cost and robust intelligent trap thru the integration of capacitive wing-beat sensor into current commercial insect electrocuting traps. It is accomplished by

incorporating the high-voltage supply into the capacitive sensing functionality. The expansion of the initial core concept in prior work has been explored by this paper through the development and testing of the proposed method. The experiment on the proposed method has yield comparable results to the prior initial work using *Culex tritaeniorhynchus* and *Aedes albopictus* samples. The preliminary results presented by this paper have introduced a new promising direction and possibility for insect detection in commercial traps.

REFERENCES

- [1]. C. M. Williams and R. Galambos, "Oscilloscopic and Stroboscopic Analysis of the Flight Sounds of *Drosophila*," *Biol. Bull.*, vol. 99, no. 2, pp. 300–307, 1950.
- [2]. L. E. Chadwick, "A Simple Stroboscopic Method for the Study of Insect Flight," *Psyche (New York)*, vol. 46, no. 1, pp. 1–8, 1939.
- [3]. J. W. S. Pringle, "The Gyroscopic Mechanism of the Halteres of Diptera," *Philos. Trans. R. Soc. B Biol. Sci.*, vol. 233, no. 602, pp. 347–384, 1948.
- [4]. M. D. R. Jones, "The automatic recording of mosquito activity," *J. Insect Physiol.*, vol. 10, no. 2, pp. 343–351, 1964.
- [5]. S. Vogel, "Flight in *Drosophila*," *J. Exp. Biol.*, vol. 46, no. 2, pp. 383–392, 1967.
- [6]. I. R. Richards, "Photoelectric Cell Observations of Insects in Flight," *Nature*, vol. 175, p. 128, Jan. 1955.
- [7]. D. F. Silva, V. M. A. Souza, D. P. W. Ellis, E. J. Keogh, and G. E. A. P. A. Batista, "Exploring Low Cost Laser Sensors to Identify Flying Insect Species: Evaluation of Machine Learning and Signal Processing Methods," *J. Intell. Robot. Syst. Theory Appl.*, vol. 80, pp. 313–330, 2015.
- [8]. G. Batista, E. Keogh, A. M. Neto, and E. Rowton, "SIGKDD demo: sensors and software to allow computational entomology, an emerging application of data mining," in *KDD '11 Proceedings of the 17th ACM SIGKDD international conference on Knowledge discovery and data mining*, 2011, pp. 761–764.
- [9]. I. Potamitis and I. Rigakis, "Novel Noise-Robust Optoacoustic Sensors to Identify Insects Through Wingbeats," *IEEE Sens. J.*, vol. 15, no. 8, pp. 4621–4631, 2015.
- [10]. I. Potamitis and I. Rigakis, "Large aperture optoelectronic devices to record and timestamp insects' Wingbeats," *IEEE Sens. J.*, vol. 16, no. 15, pp. 6053–6061, 2016.
- [11]. T. H. Ouyang, E. C. Yang, J. A. Jiang, and T. Te Lin, "Mosquito vector monitoring system based on optical wingbeat classification," *Comput. Electron. Agric.*, vol. 118, pp. 47–55, 2015.
- [12]. Y. Chen, "Mining Time Series Data: Flying Insect Classification and Detection," University of California Riverside, 2015.
- [13]. Y. Chen, A. Why, G. Batista, A. Mafra-Neto, and E. Keogh, "Flying Insect Classification with Inexpensive Sensors," *J. Insect Behav.*, vol. 27, no. 5, pp. 657–677, 2014.
- [14]. S. A. A. Rahuman, J. Veerappan, R. V. Rajesh, S. A. A. Rahuman, J. Veerappan, and R. V. Rajesh, "Classification of Flying Insects with high performance using improved DTW algorithm based on hidden Markov model," *Brazilian Arch. Biol. Technol.*, vol. 59, no. December, pp. 1–12, 2016.
- [15]. D. F. Silva, V. M. A. De Souza, G. E. A. P. A. Batista, E. Keogh, and D. P. W. Ellis, "Applying machine learning and audio analysis techniques to insect recognition in intelligent traps," in *Proceedings - 2013 12th International Conference on Machine Learning and Applications, ICMLA 2013*, 2013, vol. 1, pp. 99–104.
- [16]. Y. Qi, G. T. Cinar, V. M. A. Souza, G. E. A. P. A. Batista, Y. Wang, and J. C. Principe, "Effective insect recognition using a stacked autoencoder with maximum correntropy criterion," *Proc. Int. Jt. Conf. Neural Networks*, vol. 2015-Septe, 2015.
- [17]. K. Li and J. C. Principe, "Automatic Insect Recognition Using Optical Flight Dynamics Modeled By Kernel Adaptive Arma Network," in *2017 IEEE International Conference on Acoustics, Speech and Signal Processing (ICASSP)*, 2017, pp. 2726–2730.
- [18]. I. Potamitis and I. Rigakis, "Measuring the fundamental frequency and the harmonic properties of the wingbeat of a large number of mosquitoes in flight using 2D optoacoustic sensors," *Appl. Acoust.*, vol. 109, pp. 54–60, 2016.
- [19]. D. A. A. Santos, L. E. Teixeira, A. M. Alberti, V. Furtado, and J. J. P. C. Rodrigues, "Sensitivity and Noise Evaluation of an Optoelectronic Sensor for Mosquitoes Monitoring," in *2018 3rd International Conference on Smart and Sustainable Technologies (SpliTech)*, 2018, pp. 1–5.
- [20]. T. Brendan Khoo, M. Muralindran, R. P. Rosalyn, and W. W. Kitt, "Capacitive Mosquito Wing-beat Sensor: A Novel Sensor for Intelligent Traps," *Int. J. Eng. Res. Appl.*, vol. 10, no. 7, pp. 18–27, 2020.